Anion Photoelectron Imaging Spectroscopy of $C_6F_5X^-$ (X = F, Cl, Br, I)

Kristen Rose McGinnis,[†] Conor J. McGee,[†] Thomas Sommerfeld,[‡] and Caroline Chick Jarrold[†,*]

[†]*Department of Chemistry, Indiana University, 800 East Kirkwood Avenue, Bloomington, Indiana, 47405 USA*

[‡]*Department of Chemistry and Physics, Southeast Louisiana University, SLU 10878, Hammond, LA 70402*

ABSTRACT

The photoelectron (PE) spectra of $C_6F_5X^-$ (X = Cl, Br, I) and computational results on the anions and neutrals are presented and compared to previously reported results on $C_6F_6^-$ (*J. Phys. Chem. A* **2023**, *127*, 8556-8565). The spectra all exhibit broad, vibrationally unresolved detachment transitions, indicating that the equilibrium structures of the anions are significantly different from the neutrals. The PE spectrum of $C_6F_5Cl^-$ exhibits a parallel photoelectron angular distribution (PAD), similar to that of the previously reported $C_6F_6^-$ spectrum, while the PE spectra of $C_6F_5Br^-$ and $C_6F_5I^-$ have isotropic PADs, and also exhibit a prominent X^- PE feature due to photodissociation of $C_6F_5X^-$ resulting in X^- formation. Identification of the $C_6F_5X^-$ detachment transition origins, which is equivalent to the neutral electron affinity (EA), in all three cases is difficult, since the broadness of the detachment feature is accompanied by vanishingly small detachment cross section near the origin. Upper limits on the EAs were determined to be 1.70 eV for C_6F_5Cl, 2.10 eV for C_6F_5Br, and 2.00 eV for C_6F_5I, all significantly higher than the 0.76 eV upper limit determined for C_6F_6 with the same experiment. The broad detachment transitions are consistent with computational results, which predict very large differences between the neutral and anionic C–X (X = Cl, Br, I) bond lengths. Based on differences between the MBIS atom charges in the anions and neutrals, the excess charge in the anion is on the unique C atom and X, in contrast to the non-planar C_{2v} structured $C_6F_6^-$ anion, for which the charge is delocalized over the molecule. In $C_6F_5Cl^-$, the C–Cl bond is predicted to be bent out of the plane, while both $C_6F_5Br^-$ and $C_6F_5I^-$ are predicted to be planar. The impact of the interruption of the symmetry in the hexafluorobenzene neutral and anion on the molecular and electronic structure of $C_6F_5X/C_6F_5X^-$ is considered, as well as the possible dissociative state leading to X^- (X = Br, I) formation, and the nature of the C–X bond.

*Author to whom correspondence should be addressed. Electronic mail: cjarrold@indiana.edu

1. INTRODUCTION

Small closed-shell organic molecules generally do not form stable negative ions unless they have electron-withdrawing substituents, such as carbonyl groups,[1–5] halogens,[6–13] cyano groups,[14] or nitro groups.[1516] In contrast with larger, non-substituted polycyclic hydrocarbons,[17–23] which can support an excess electron occupying what would correspond to the delocalized LUMO of the neutral, the charge in smaller, substituted molecules can be more localized, with a substantial impact on the structure of the anion relative to the neutral. For example, ethanedial, or glyoxal (HCOCHO) can form a stable anion in which the excess charge is in an out-of-plane π orbital that is C–C bonding and C=O antibonding, resulting in an anion with significantly different C–O and C–C bond lengths relative to the corresponding neutral.[1,4]

In this report, we focus on the electronic and molecular structures of halopentafluorobenzene anions and neutrals. To place this current study in context, a number of groups have implemented electron attachment/thermal detachment methods[24–30] to measure the electron affinity (EA) of C_6F_6, the tortuous history of which was concisely detailed by Miller *et al*.[26] A complementary approach for determining the EA is photoelectron (PE) spectroscopy of $C_6F_6^-$,[7,31–36] in which the stable negative ion is isolated and photodetached using a fixed frequency laser, and electron kinetic energy (e^-KE) analysis is conducted to determine the relative energies of anion and neutral states. In both techniques, the significant difference in the structures of the anion (non-planar C_{2v} symmetry) and associated neutral (D_{6h} symmetry) necessitates a measure of caution when determining the adiabatic EA from the data. In the case of the anion PE spectrum, the transition origin, from which the EA is determined, may have near-zero intensity because of low Franck-Condon overlap between the anion and neutral ground states.

The EAs of perfluorophenyl compounds, C_6F_5X have also been studied previously using electron attachment methods.[37,38] Dillow and Kebarle reported the free energies for electron capture of C_6F_5X (X = F, Cl, Br, I) to be -0.646 eV, -0.880 eV, -1.214 eV, and -1.48 eV, respectively.[37] The values determined for X = F and Cl tracked with the EA values of C_6F_6 and C_6F_5Cl of 0.53 eV and 0.75 eV, respectively, determined by Viggiano and coworkers using electron attachment/thermal detachment.[26]

Our group has used anion PE spectroscopy to study a series of fluorinated benzenes and phenyl radicals. As a follow-up on a previous report of the EA of C_6HF_5,[34] we present the PE spectra of $C_6F_5X^-$ (X = Cl, Br, I). The lower symmetry of $C_6F_5X^-$ compared to $C_6F_6^-$ leads to the possibility of electron localization in the unique C–X bond, and therefore very different PE spectra. Indeed, Bowen and coworkers[39] recently reported the PE spectrum of $C_6F_5I^-$ measured using 3.49 eV and 4.66 eV photon energies, and while the spectrum reported here shows subtle differences with Bowen's that we explain below, the results do confirm striking differences between $C_6F_6^-$ and $C_6F_5I^-$.

As will be described below, the PE spectrum of $C_6F_5Cl^-$ is qualitatively similar to the PE spectrum of $C_6F_6^-$ published previously in that it exhibits a broad detachment transition and a parallel photoelectron angular distribution (PAD). However, the detachment transition observed in the PE spectrum of $C_6F_5Cl^-$ is significantly higher in energy than that of $C_6F_6^-$. The PE spectra of $C_6F_5X^-$ (X = Br, I) show pronounced, narrow transitions due to X^- photodetachment, superimposed on a lower-intensity broad band attributed to direct detachment of the intact $C_6F_5X^-$ (X = Br, I) anions. The direct detachment transitions in these spectra have PADs that are isotropic, and therefore different from those observed in the PE spectra of $C_6F_6^-$ and $C_6F_5Cl^-$. We demonstrate that the Br^- signal is due to a two-photon process, in which the first photon photodissociates the anion forming the Br^- anion and remnant $\cdot C_6F_5$ radical neutral:

$$C_6F_5Br^- + h\nu \longrightarrow \cdot C_6F_5 + Br^- \quad (1)$$

$$Br^- + h\nu \longrightarrow Br + e^- \quad (2)$$

I^- formation during the photodetachment of $C_6F_5I^-$ does not show a clear power-dependence expected for a two-photon process, which we attempt to rationalize in the context of other experimental observations and computational results.

2. METHODS

2.1. Experimental Details. The experiments were conducted using an anion PE imaging apparatus described previously.[40] Briefly, the $C_6F_5X^-$ (X = Cl, Br, I) anions were generated using a photoemission source.[7] The neutral precursors (C_6F_5Cl from Sigma-Aldrich, 99% purity; C_6F_5Br from Sigma-Aldrich, 99% purity, and C_6F_5I from Sigma-Aldrich, 99% purity) individually seeded in ultra-high purity helium maintained at 80 psig, were injected into a vacuum chamber using a pulsed molecular beam valve operating at 30 Hz. To boost the ion signal, the gas manifold was heated modestly with a heating tape until the signal reached satisfactory levels. The gas mixture passed over a Gd_2O_3 pressed powder surface (the photoemitter), while 1.3 mJ/pulse of a second harmonic (532 nm, or 2.330 eV) output of a Nd:YAG impinged on the surface. The neutral molecules attached the resulting low-energy photoelectrons forming anions that then thermalized in the He buffer gas.

The gas mixture passed through a skimmer, and anions separated by *m/z* in a 0.97-m Bakker-style[41,42] beam-modulated time-of-flight mass spectrometer. The ions then drifted through a laser interaction region prior to colliding with a dual microchannel plate detector assembly. Mass spectra were recorded for each sample. The resolution is sensitive to settings in the experiment, but $m/\Delta m$ is typically between 150 and 300.

As the mass separated anions passed through the laser interaction region, they were selectively photodetached with a second Nd:YAG laser timed to intersect only the anion of interest. The photoelectrons were energy analyzed using a velocity map imaging setup.[43,44,45] Images generated on a 70-mm dual microchannel plate/phosphor screen detector assembly were recorded by a CCD camera, and accumulated using the NuACQ 0.9 program provide by the Suits group.[46] The three-dimensional velocity distributions were extracted from the two-dimensional images using the BASEX[47] and pBASEX programs.[48] Velocities, proportional to the radii of the annular images generated in this experiment, were converted to e^-KE, calibrated using the well-known spectrum of O_2^-.[49] The instrumental resolution, $\Delta e^-KE/e^-KE$ is 2.5%.

The e^-KE is governed by the photon energy, $h\nu$, the EA of the neutral, and the internal energy distributions of the initial anion (E_{int}^{anion}) and final neutral ($E_{int}^{neutral}$) states via:

$$e^-KE = h\nu - EA - E_{int}^{neutral} + E_{int}^{anion} \quad (3)$$

If the anions are internally cold, $E_{int}^{anion} \approx 0$, and the e^-KE distribution reflects the final state distribution of the neutral. In practice, the temperature of the anions is non-zero, and internal energy introduces some spectral congestion.

The spectra presented here are presented as relative electron yield versus electron binding energy, e^-BE:

$$e^-BE = h\nu - e^-KE \quad (4)$$

The e^-BE values are independent of the photon energy used and equal the energies of the final neutral state(s) relative to the initial anion state(s).

The PADs can be determined directly from the images (raw and reconstructed images are included in the **Supporting Information**). For the sake of simplicity, we used the zero and second-order coefficients from the Legendre polynomial reconstruction of the images in pBASEX to resolve the relative PE yields ejected parallel and perpendicular to the electric field vector of the detachment laser.

Spectra were collected using both 355 nm (3.495 eV) and 532 nm (2.330 eV) wavelengths. The images were collected for $C_6F_5X^-$ (X = Cl, Br, I) at 3.495 eV with 196,200, 160,200, and 324,00 shots respectively. The spectra collected using 2.330 eV photon energy provided limited information, showing only the threshold signal in the PE spectra of $C_6F_5Br^-$ and $C_6F_5I^-$. No signal was observed for $C_6F_5Cl^-$ using 2.330 eV photon energy, which is consistent with the PAD, as will be described below.

2.2. Computational Details. To determine how sensitive the computational results are to the method used over a set of systems that include much heavier elements, a series of calculations were done on all three anions and neutrals using the ωB97X functional[50] with the def2-TZVPPD (def2-ECP for I)[51–53] basis, with the domain-based local pair neutral orbital (DLPNO)-CCSD(T)/aug-cc-pVTZ[54] single-point calculations[55] on the ωB97X-optimized structures, along with B2GBLYP/aug-cc-pVTZ (SK-MCDHF-

RSC ECP for Br and I)[56] calculations, with DLPNO-CCSD(T)/aug-cc-pVTZ (SK-MCDHF-RSC ECP for Br and I) single-point calculations on the B2GBLYP-optimized structures. These calculations were performed using version 5.0.4 of the ORCA electronic structure computational software package.[57]

Minimal Basis Iterative Stockholder (MBIS)[58] atom charges were calculated and are included in the **Supporting Information**. They provide qualitative insight into charge localization in anions.[59] Loewden spin populations were additionally computed for the doublet anions using from B2GBLYP/aug-cc-pVTZ results.

To compare computational and experimental results, the adiabatic EAs of each neutral were calculated as the difference between the optimized, zero-point-corrected energies of the neutral and associated anion. In addition, the vertical detachment energy (VDE), which generally (but not always) corresponds to the energy at which the detachment band reaches maximum intensity, is calculated as the energy between the neutral constrained to the optimized anion, and the anion itself. The VDE – EA difference, in general, reflects the breadth of the Franck-Condon manifold. The larger the difference, the broader the transition is predicted to be.

For the purpose of directly comparing computational results on C_6F_5X with previously reported results on C_6F_6 neutrals and anions[34] using the same method, basis set, and electronic structure code, additional calculations on the C_6F_5Cl and C_6F_5Br neutrals and anions were done using the Becke, 3-parameter, Lee, Yang, and Parr (B3LYP) functional[60-62] and the diffuse Dunning-style correlation[54,63,64] consistent triple zeta (aug-cc-pVTZ) basis set, within the Gaussian 16 suite for electronic structure calculations.[65] Results from these calculations including APT charges are presented in the **Supporting Information**, and are consistent with the results from methods described above.

3. RESULTS AND DISCUSSION

3.1. Mass Spectra of Anions Generated from C_6F_5X (X = CH_3, Cl, Br, I).

Mass distributions of the negative ions generated by passing the neutral C_6F_5X (X = Cl, Br, I) seeded in ultra-high purity He through the photoemission source are shown in Figure 1. Intact anions were

observed for all three molecules, along with pentafluorophenyl anion ($C_6F_5^-$). X^- (X = I, Br) is observed in the mass spectra of anions generated from C_6F_5Br and C_6F_5I. Cl^- does not appear in the $C_6F_5Cl^-$ mass spectrum because it was excluded by the settings used to optimize signal in the *m*/*z* ranges shown.

The mass spectra of ions generated from all three molecules also show anions generated through loss of –F. However, because no $C_6F_nX^-$ ($n < 5$) anions are observed, F loss occurs only after X loss. Ions generated from residual C_6F_5Br are present in both $C_6F_5Cl^-$ and $C_6F_5I^-$ mass spectra. GdF_4^- is observed in all three panels, and is likely the result of minor ablation of the Gd_2O_3 photoemission target, followed by reactions with fluorine atoms or with the C_6F_5X molecules.

We do not observe evidence of dissociation of the anions in the acceleration stack as we have observed in previous studies on similar systems.[66] On this basis, we infer that all fragmentation occurs in the source or in the *ca.* 100 μs prior to acceleration into the mass spectrometer.

3.2. PE spectra of $C_6F_5X^-$ (X = F, Cl, Br, I).

Figure 2 shows the anion PE spectra of (a) $C_6F_5Cl^-$, (b) $C_6F_5Br^-$ and (c) $C_6F_5I^-$, respectively. These spectra were obtained using 3.495 eV photon energy. The darker blue traces reflect the relative electron yields ejected parallel to the electric field vector of the incident photon, and the light blue traces reflect the relative electron yields ejected perpendicular. The previously reported[33] PE spectrum of $C_6F_6^-$ obtained using the same instrument and ion source is shown in Figure 2(a) (dotted red and orange traces representing the relative parallel and perpendicular yields, respectively) superimposed on the PE spectrum of $C_6F_5Cl^-$ for direct comparison. The raw and reconstructed images are included in the **Supporting Information**.

General features. While the photoelectron angular distributions (PADs) determined from the reconstructed images and reflected in the parallel and perpendicular traces will be discussed further below, we first describe the main features in the spectra. Each exhibits a broad transition appearing between 2.00 and 3.49 eV. The spectra of $C_6F_5Br^-$ and $C_6F_5I^-$, show distinctive narrow atomic detachment signal due to Br^- (3.36 eV) and I^- (3.06 eV), respectively. The presence of this atomic signal indicates fragmentation is

occurring, most likely via photodissociation of the anion, as there is no evidence in the mass spectra of dissociation while ions are accelerating into the instrument (*vide supra*).

The $C_6F_5Cl^-$ PE spectrum has a profile that appears similarly broad to the $C_6F_6^-$ spectrum, though the VDE is 1.40 eV higher in binding energy.

Because the detachment transitions are very broad, the origin of the transitions might not be observable in the spectra due to vanishingly small Franck-Condon overlap. Instead, we determine an upper limit of the origin to be 1.7 eV for $C_6F_5Cl^-$, 2.10 eV for $C_6F_5Br^-$, and 2.00 eV $C_6F_5I^-$. These values are based on the e^-BE at which the detachment signal becomes distinct from the baseline noise level, and are significantly higher than measurements made using different methods,[26,37] as well as computed adiabatic EAs (*vide infra*), which again points to the likelihood of zero Franck-Condon overlap near the origin. In the case of $C_6F_5Br^-$ and $C_6F_5I^-$, the upper limits were determined from the spectra measured using 2.330 eV shown in the **Supporting Information**. The VDE determined from the $C_6F_5Cl^-$ PE spectrum is 2.95 ± 0.05 eV. The VDE values for the $C_6F_5Br^-$ and $C_6F_5I^-$ spectra are difficult to determine because of the atomic detachment features, but we estimate them both to be between 3.15 eV and 3.45 eV, based on the spectra integrated over all angles (**Supporting Information**).

We note here that the PE spectrum of $C_6F_5I^-$ reported here is in agreement with the spectrum reported by Bowen and coworkers[39] obtained with the same photon energy, with two distinctions. First, Bowen's spectrum also exhibited a spectroscopic feature attributed to $C_6F_5^-$, supported by their spectrum of *m/z*-isolated $C_6F_5^-$. Our spectrum does not exhibit this distinct $C_6F_5^-$ feature, which could be attributed to differences in detachment laser powers and/or source conditions. Second, the intensity of the I^- detachment feature relative to the $C_6F_5I^-$ detachment feature is lower in the spectrum reported by Bowen and coworkers than the spectrum presented here. New information determined from the spectrum presented here is the isotropic PAD.

Variation of X^- signal intensity with detachment power. Detachment laser power studies were conducted to determine whether the X^- anions evident in the PE spectra of $C_6F_5Br^-$ and $C_6F_5I^-$ were

generated by photodissociation followed by photodetachment of X^- [Equations (1) and (2) shown above] ***or*** by delayed dissociation ion the ion beam (which we infer is unlikely, *vide supra*):

$$C_6F_5X^- \xrightarrow{\tau} \cdot C_6F_5 + X^- \qquad (5)$$

The assumption in this case would be that X^- generated by delayed dissociation would continue drifting with nearly the same velocity as the original $C_6F_5X^-$ ion packet, and would then be detached by a simple one-photon process,

$$\cdot C_6F_5 + X^- + h\nu \rightarrow \cdot C_6F_5 + X + e^- \qquad (6)$$

If the former, a two-photon process is involved, and the intensity of the X^- detachment feature should vary with the square of the detachment power. If the latter process is involved, the X^- signal is a from a one-photon process. The intensity of the X^- feature would therefore change linearly with laser power.

Figure 3 shows the ratio of the integrated Br^- or I^- peak intensity to the integral of the broad feature, which we attribute to the direct detachment of the intact anion, plotted against the normalized laser fluence (actual values ranged from 0.33 J cm^{-2} to 1.21 J cm^{-2}). Uncertainties arise from identifying the baseline of the X^- signal superimposed on the direct detachment signal due to signal to noise. The data are plotted in this manner to eliminate variations due to changes in ion signal over the course of the measurements, and it additionally factors out the linear dependence of the direct detachment (one-photon) signal. If the Br^- or I^- features were due to a one-electron transition, i.e., if free Br^- and I^- atomic ions were formed by a delayed dissociative attachment process in the ion beam after being accelerated into the mass spectrometer [Eqs. (5) and (6)], the ratio of the intensity of the atomic anion detachment features to the broad detachment signal would not change with the laser power, and the plots would show horizontal lines. Instead, the Br^- signal increases unambiguously (if not perfectly linearly) with laser power, indicating that the photodissociation followed by Br^- detachment (within one laser pulse) is occurring.

In the case of $C_6F_5I^-$, the ratio of I^- signal intensity to $C_6F_5I^-$ signal does appear to increase at the lowest laser powers, but flattens and appears to decrease with higher powers, so is not well-fit with a linear regression. This effect suggests that at higher powers, stimulated emission from the dissociative excited

state of $C_6F_5I^-$ repopulates the ground state of the anion, thereby increasing the proportion of signal attributable to direct detachment of the bound anion.

We note here that the absence of signal due to Cl^- in the PE spectrum of $C_6F_5Cl^-$ is not an indication that this anion does not undergo a dissociative process, since the EA of Cl is higher than the photon energy used; Cl^- detachment signal would therefore not be observed if Cl^- anions were generated.

The absence of $\cdot C_6F_5^-$ detachment signal in any of the spectra will be addressed in the discussion section.

PADs. Referring back to Figure 2, the broad transitions in both the PE spectra of $C_6F_5Cl^-$ and $C_6F_6^-$ (from Ref. 34) have distinctly parallel PADs, though the signal becomes isotropic approaching the high e^-BE limit in the $C_6F_5Cl^-$ spectrum. In contrast, the spectra of $C_6F_5Br^-$ and $C_6F_5I^-$ are isotropic. The PAD is governed by the symmetry of the orbital associated with the detachment transition. Isotropic PADs are indicative of $l = 0$ outgoing PE waves (s-waves) and are consistent with near-threshold detachment of electrons from atomic p-like orbitals.[67-71] Transitions yielding s-waves have non-zero cross section near threshold,[72] and indeed, signal is observed at and above 2.0 eV in the PE spectra of $C_6F_5Br^-$ and $C_6F_5I^-$ measured with 2.330 eV photon energy (**Supporting Information**). In contrast, the parallel PAD exhibited in the PE images and spectrum of $C_6F_5Cl^-$ is indicative of $l = 1$ outgoing PE waves (p-waves), which, per the Wigner threshold law,[72] would have vanishingly small photodetachment cross section near threshold. Consistently, no electron signal was observed when we attempted to collect the spectrum of $C_6F_5Cl^-$ using 2.330 eV photon energy.

To better understand the significant differences between the spectra of $C_6F_5Cl^-$ and $C_6F_5X^-$ (X = Br, I), both in terms of the overall appearance and the PADs, we consider the computational results.

3.3. Computational Results

In this section, we compare the results of the computed molecular and electronic structures of the anionic and neutral $C_6F_5X^-$ along the X = F, Cl, Br, and I series. A feature of the calculations to bear in mind is that the basis sets necessarily change across this series, as described in the computational methods

section. The valence shells are consistent, but core electrons for some Br and all I calculations are treated using a relativistic ECP, as detailed in the methods section.

Molecular Structures. The optimized molecular structures of neutral and anionic C_6F_5X (X = F, Cl, Br, I) computed using the ωB97X functional are shown in Figure 4. More details on the individual bond lengths and angles for C_6F_5X (X = F, Cl, Br, I) neutrals and anions using ωB97X/def2-TZVPPD (def2-ECP for I) and B3LYP/aug-cc-pVTZ and C_6F_5X (X = F, Cl, Br, for the purpose of direct comparison with previously reported results[34] on $C_6F_6/C_6F_6^-$) are included in the **Supporting Information.**

The neutral structures are all predicted to be planar, and shown the expected increase in C–X bond length along the X = F, Cl, Br, I series, with the largest difference being between F and Cl.

The structure of $C_6F_6^-$ reported here is consistent with previous reports:[7,31,32,34] All C–F bonds are bent out of the C_6 plane (two *para* –F atoms more dramatically so in one direction, the other four –F atoms in the opposite direction), forming a C_{2v} structure shown in Figure 4(a). The two identical C–F bonds are elongated in the anion relative to the neutral by 0.062 Å. In contrast, The C–X bonds in the $C_6F_5X^-$ (X = Cl, Br, I) anions are substantially longer relative to the C–X bond in neutral C_6F_5X (*ca*. 0.7 Å). The C–Cl bond in $C_6F_5Cl^-$ is predicted to be bent out of the plane by 24°.

The optimized structures of $C_6F_5Br^-$ and $C_6F_5I^-$, while showing a small (< 5°) C–X bend out of the plane, can be taken to be planar on average and floppy. For example, the barrier for the C–Br bond to bend from one side of the plane to the other is 7 cm^{-1}, and the bend frequency is 14 cm^{-1}, so the vibrational wavefunction would span both (shallow) wells and the transition region. By comparison, the barrier in $C_6F_5Cl^-$, the barrier is 255 cm^{-1}, and the local C–Cl bend frequency is 52 cm^{-1}. The structure is therefore definitively non-planar, per calculations. Planarity versus non-planarity among these congeners is governed by the overlap between the *n*p orbitals on X and the bonding orbitals associated with the C_6F_5 portion of the anion.

Beyond the C–X bond, the C–F bonds in the $C_6F_5X^-$ (X = Cl, Br, I) anions are elongated 0.02-0.03 Å compared to the neutral. The C–C bonds adjacent to the C–X are shorter by 0.02 Å in the anion.

Otherwise, the C_6F_5 portion of the molecules are relatively unchanged across the X = Cl, Br, I series and between the anions and neutrals. More details on the structures are included in the **Supporting Information.**

The broadness of the detachment transitions observed in the PE spectra of $C_6F_5X^-$ (X = Cl, Br, I) can therefore be attributed to the dramatic difference between the anion and neutral in C–X bond length. The neutral C_6F_5X molecule prepared by detachment of the $C_6F_5X^-$ anion is in a distribution of highly vibrationally excited levels of the C–X stretch mode. The PE spectrum of $C_6F_5Cl^-$ is further congested by the C–Cl out-of-plane bend activation upon detachment. The breadth of the $C_6F_6^-$ PE spectrum, in contrast, is due to overall delocalized structural differences between the neutral and anion.

Electronic Structures. Table 1 summarizes the adiabatic EA and VDE values computed for the $C_6F_5X^-$ photodetachment transitions using the methods described above, along with the experimental values from this study. While there are small variations in the transition energies computed using the different methods, a general trend is that the EAs increase from approximately 0.4 eV for $C_6F_6^-$, 0.7 eV for $C_6F_5Cl^-$, 1 eV for $C_6F_5Br^-$, to 1.3 – 1.4 eV for $C_6F_5I^-$.

A more striking difference is the change in VDE values between X = F and X = Cl, Br. The difference between the compute VDE and EA values computed for $C_6F_6^-$ are approximately 1 eV. In contrast, the VDE values are predicted to be approximately 2 eV higher than the EA values for $C_6F_5Cl^-$ and $C_6F_5Br^-$. This indicates that the respective neutrals are prepared with 2 eV of internal energy (primarily in the C–X stretching mode, as noted above) at the most intense point in the spectrum. For $C_6F_5I^-$, the VDE – EA difference is smaller (1.5 eV to 1.8 eV, depending on the method), but is still in line with a very broad spectrum, and suggests that indeed the upper limits on the EA determined experimentally are significantly higher than the actual EA. The single-point VDE values predicted for $C_6F_5Cl^-$ with DLPNO-CCSD(T), 2.96 eV or 2.82 eV depending on the method used to optimize the structure, are in good agreement with the observed value (2.95 eV), which provides some validation of the computationally determined EA values of 0.68 to 0.70 eV with the same methods.

Figure 5 shows depictions of the molecular orbitals and computed relative energies from B3LYP/def2-SVP for (a) $C_6F_6^-$, (b) $C_6F_5Cl^-$, (c) $C_6F_5Br^-$, and (d) $C_6F_5I^-$ optimized using ωB97X/def2-TZVPPD (def2-ECP for I). Note that the orbital energies should be taken with the appropriate grain of salt, but they provide a qualitative picture of the differences and similarities of the electronic structures across the X = F, Cl, Br, I series. The primarily in-plane (with the exception of the C–Cl bond in $C_6F_5Cl^-$) σ orbital energies are indicated by the red lines and the out-of-plane π orbital energies are indicated by the blue lines.

The most obvious differences between the electronic structures of $C_6F_6^-$ and $C_6F_5X^-$ (X = Cl, Br, I) lie in the frontier orbitals due to the localization of X *n*p orbitals in the molecular anions, and the relative energies of these orbitals compared to C–F bonding and antibonding orbitals. As shown previously,[7,34] the singly occupied molecular orbital (SOMO) in $C_6F_6^-$ is delocalized over the C_{2v} molecule in an orbital that can be described as a hybrid of the totally symmetric σ^*_{C-F} orbital (the lowest unoccupied molecular orbital, or LUMO, in the C_6F_6 neutral) and the π_4 orbital (LUMO + 1 in the neutral) enabled by the distortion to the non-planar structure. In sharp contrast, the SOMO of $C_6F_5X^-$ (X = Cl, Br, I) anions is a distinctly localized σ^*_{C-X} orbital.

Along the $C_6F_5X^-$ (X = Cl, Br, I) series, the anions have qualitatively similar orbital occupancies and relative energies of the respective frontier orbitals, beyond the SOMOs. Lying close in energy are doubly-occupied MOs that can be largely described as nearly degenerate X *n*p orbitals orthogonal to the C–X bond. The *n*p orbital that is near perpendicular to the C_6F_5 plane is predicted to be modestly delocalized into the π system with C–X and C–F antibonding character, the latter being consistent with elongated C–F bonds in the anion relative to the neutral.

More deeply bound relative to the MOs with significant *n*p character are orbitals that correlate to the π_2 and π_3 e_{1g} degenerate orbitals in benzene, which have C–C bonding and C–X bonding character in $C_6F_5X^-$. These orbitals are not degenerate in the C_s anion or C_{2v} neutral C_6F_5X molecules, but are close-lying.

The C–X σ bonding orbital [σ_{C-X} in Figure 5(b), (c) and (d)] lies energetically between the π_1 and π_2/π_3 orbitals, and shows large contributions from the X *n*p orbital aligned with the C–X bond. This is very distinct from C_6F_6, in which all six C–F σ bonds are inner-valence, and lie below the six π_i^{C-F} orbitals shown near the bottom of Figure 5(a). Overall, the C–X bond order in the $C_6F_5X^-$ (X = Cl, Br, I) is ½. The orbital labeled π_3 and out-of-plane X *n*p orbitals represent a bonding and antibonding pair, and the SOMO counteracts the doubly-occupied σ_{C-X} bond. As with $C_6F_6^-$, the orbitals that can be described as the five bonding C–F π orbitals in $C_6F_5X^-$ (π_i^{C-X}) lie much lower in energy, reflecting the strength of the C–F bond relative to C–X (X = Cl, Br, I).

4. Discussion

The previous section reported and analyzed the experimental PE spectra and transition energies of the $C_6F_5X^-$ (X = Cl, Br, I) anions, the PADs exhibited in the anion PE spectra, and the appearance of Br^- and I^- detachment transitions observed in the PE spectra of $C_6F_5Br^-$ and $C_6F_5I^-$, with comparisons to previous results on $C_6F_6^-$. Additional comparisons were made between the electronic and molecular structures of C_6F_5X (X = F, Cl, Br, I) neutrals and anions based on computational results. Here we explore several of the nuances from these results.

Differences in Molecular Structures, Electronic Structures, and PADs. The motivation for this study was to determine the impact of interrupting the symmetry of C_6F_6 (neutral and anion) with a chemically similar, electron-withdrawing substituent. Along the $C_6F_5X^-$ (X = Cl, Br, I) series, the calculations predict that the $C_6F_5Cl^-$ anion is distorted to a C_s non-planar structure, and is most analogous to $C_6F_6^-$ in terms of the PAD determined from the PE spectra [Figure 1(a)]. Unlike $C_6F_6^-$, the effect of the non-planarity of $C_6F_5Cl^-$ is not reflected in the appearance of the SOMO [Figure 5(b)], but the lower energy π_1 orbital shows modest C–Cl bonding character enabled by the non-planarity, which is not seen in the π_1 orbitals of $C_6F_5Br^-$ or $C_6F_5I^-$.

For all three C_6F_5X (X = Cl, Br, I) neutrals and anions, the C–X bonding orbitals (σ_{C-X} and π_2) are well-separated from the C–F bonding orbitals in the same molecules (π_i^{C-F}, and the inner-valence σ_{C-F} orbitals not shown in Figure 5). The clustering C–X bonding and antibonding orbitals underpins the low-lying dissociative states in the anion, discussed below.

An important point of comparison between the experimental spectra and the computational results lies in the PADs. The isotropic appearance of the direct $C_6F_5X^-$ detachment transitions for X = Br and I reflects a purely s-wave detachment, consistent with detachment from an atomic-like *n*p orbital. The SOMOs depicted for $C_6F_5Cl^-$, $C_6F_5Br^-$ and $C_6F_5I^-$ in Figure 5(b), (c) and (d) are not isolated *n*p, as they are delocalized to some extent (*vide infra*) into the electron deficient C_6 ring, but they are similar in appearance and would suggest similar PAD. However, the C–Cl bond, and therefore the SOMO of $C_6F_5Cl^-$ is significantly bent out of plane. While not an entirely satisfactory explanation for the difference in PADs, symmetry underpins PAD, and the orientation of the 3p-like SOMO relative to the in $C_6F_5Cl^-$ is distinct from the 4p and 5p orbitals in the $C_6F_5Br^-$ and $C_6F_5I^-$ congeners.

$C_6F_5Br^-$ and $C_6F_5I^-$ photodissociation. Figure 6 shows schematics of the neutral C_6F_5X energy relative to the $\cdot C_6F_5$ + X dissociation limit[73] (all of which are higher than the C_6H_5–X bond dissociation energies)[74] along with the anionic $C_6F_5^-$ + X and $\cdot C_6F_5$ + X^- dissociation limits relative to $C_6F_5X^-$ for X = (a) Cl, (b) Br, and (c) I. The neutral and anionic energies of the intact molecules are offset by the computed EA values from this study, while the dissociation limits of the neutral and anion are offset by the known EAs of the fragments, summarized in Table 2.[39,75,76] From Figure 6(c), both the $C_6F_5^-$ + I and $\cdot C_6F_5$ + I^- dissociation limits are lower in energy than the neutral C_6F_5I + free electron limit, though intact $C_6F_5I^-$ formation is lowest in energy.

Further considering $C_6F_5I^-$, $C_6F_5^-$ + I is a lower-energy dissociation channel than the observed $\cdot C_6F_5$ + I^- channel. For both X = Cl and Br, $\cdot C_6F_5$ + X^- formation is the lower energy dissociation channel because the EAs of Cl and Br are both higher than the EA of $\cdot C_6F_5$. However, in all three cases, both photodissociation channels are energetically accessible with the 3.495 eV photon energy used for

photodetachment in this study. Note that the $C_6F_5X^- \rightarrow C_6F_4X + F^-$ dissociation channel is *ca.* 4 eV for X = Cl, and up to 4.5 eV for X = I, assuming the computed EA values are valid, so the absence of F^- detachment signal in the PE spectra is expected.

The fact that we observe no evidence of $C_6F_5^-$ photodetachment signal in any of the three spectra, combined with the observation of Br^- and I^-, suggests that the dissociative state involves promotion of an electron to the σ^*_{C-X} orbital (the SOMO). $C_6F_5Br^-$ and $C_6F_5I^-$ are C_{2v} molecules (on average, *vide supra*) with $^2A_1$ ground states. Therefore, promotion of an electron from an a_1, b_1, or b_2 orbital to the a_1 SOMO would be dipole-allowed. All valance orbitals from the π_1 to the X *n*p orbitals, excluding the respective π_3 orbitals, fall into this category. We will not speculate further on which transition(s) might be involved, beyond suggesting that promotion of electrons from an *n*p non-bonding orbital to the SOMO would create a hole in the *n*p shell, which is not conducive to X^- (np^6) formation. Therefore, likely candidates would be promotion of an electron from the π_2 orbital, resulting in a $^2B_1$ dissociative state, or from the σ_{C-X} orbital, resulting in a $^2A_1$ dissociative state.

It seems likely that analogous transitions involved in the appearance of both Br^- and I^- in the spectra of their respective parent ions, given the similarity between the molecular orbital occupancies and relative energies computed and presented in Figure 5. However, the disparity in the results of the detachment power study does suggest some differences between the two. Studies that measure the kinetic energy release of the photofragments, such as those done in the Continetti group,[77-80] would shed more light on the dissociation process.

As a final comment on Figure 6, the C–X BDEs shown in the diagrams are based on Ref. 73, and the EA values of C_6F_5X are based on the computational results presented here. From these computed values and the known EAs of X, C–X bond dissociation energies for the anions are approximately one half of the neutral C–X bond dissociation energy, or less. In this set of systems, the bond order tracks with the BDE in what appears to be a straightforward manner.

The nature of the C–X bond in C_6F_5X The C–X bond is well known to be polar with the halobenzenes (C_6H_5X) having similar experimentally-determined dipole moments ranging from 1.6 to 1.7 Debye.[81] The polar bond can be rationalized based on differences in the electronegativities of C and X.[82] In the case of C_6F_5X (X = Cl, Br, I), the question of whether the C–X bond is similarly polar is interesting because the EA of the $\cdot C_6F_5$ radical (*ca*. 3.2 eV),[39,75] which factors into the Mulliken definition of electronegativity,[83] is comparable to the EAs of X = Cl, Br, and I.

To further explore the nature of the C–X bond in C_6F_5X (X = Cl, Br, I) molecules, we consider (1) atomic charges, (2) spin populations (SP), and (3) dipole moments, all of which are determined computationally.

While computed atomic charges, like orbital energies, are another computational result that should be taken with the appropriate grain of salt, differences among computed charges can be instructive. The MBIS atom charge for the carbon atom bound to X (C_X) along with the MBIS atom charge of X for the C_6F_5X (X = F, Cl, Br, I) neutrals and anions are summarized in Table 3 (all MBIS atom charges along with APT charges for comparison are included in the **Supporting Information**).

The overall relative charges suggest that the C–X (X = Cl, Br, I) bond is less polar than the C–F bond in the neutrals. The MBIS atom charges computed for C_X trends from positive to increasingly negative along the F, Cl, Br, I series, while the MBIS atom charge on X trends from negative to positive along the same series. For X = Cl, Br, and I, the C_X center is less positively charged than the C atoms bound to F (particularly those adjacent to C_X), and the X molecule in the neutral has a smaller negative charge than the F atoms.

The MBIS atom charges computed for the anion suggest the X atom assumes a significantly more negative charge than the F atoms. A useful comparison is the difference between the anion and neutral MBIS atom charges, also included in Table 3. The difference between the MBIS atom charges on the F centers between the anion and neutral C_6F_5X (X = Cl, Br, I) is small, *ca*. -0.05 (slightly more negative in the anion) relative to the difference for X, *ca*. -0.6 (significantly more negative in the anion), which is

consistent with the molecular orbital picture of the neutral SOMO being the σ^*_{C-X} orbital. Among the X = Cl, Br, I series, the $C_6F_5Cl^-$ has the excess charge more delocalized to the C_X and F atoms. The difference is not dramatic, but it does align with a distinction between these three anions.

As a second consideration, the anion is in a doublet state. Therefore, the Loewdin SPs, also included in Table 3, reflect where the unpaired, excess electron is localized. In the case of $C_6F_5X^-$ (X = Cl, Br, I) is split fairly evenly between C_X and X, with the trend of increasing SP on X along the X = Cl, Br, and X series.

The third consideration involves the computed dipole moments of the C_6F_5X neutrals, which show the trend of decreasing C–X bond polarity from X = Cl to X = I. By symmetry, the dipole moment of C_6F_6 is zero. The results of B2GBLYP calculations predict the dipole moment for C_6F_5Cl to be 0.35 D, 0.64 D for C_6F_5Br, and 0.98 D for C_6F_5I (these values and those computed using ωB97X, along with figures indicating the dipole vector, are included in the **Supporting Information**). This trend reflects the smaller negative charge localized on X relative to the F substituents, and therefore a less polar C–X bond.

Taken together, the C–X bond in neutral C_6F_5X (X = Cl, Br, I) is less polar than the C–F bonds, and less polar than the C–X bond in C_6H_5X. The C–I bond, which is the least polar, is also the weakest due to the relatively poor orbital overlap.

As noted above, the difference in electronegativity is typically invoked to characterize the bond type (ionic, polar, covalent). However, hybridization has been shown to influence different parameters of molecules, including electronegativity (Bent's Rule).[84] Cao *et al*. also found that the bond energies of $C(sp^3)$–X and $C(sp^2)$–X were different due to a difference in hybridization leading to a difference in electronegativities.[85] In this study, the electron depletion of C-centers (due to the C–F bond) adjacent to the C–X bond also impacts the electronegativity of this C center, and therefore the nature of the bond.

4. CONCLUSIONS

The PE spectra of $C_6F_5X^-$ (X = Cl, Br, I) and computational results on the anions and their associated neutrals were presented and analyzed. The broad, vibrationally unresolved detachment transitions observed in the spectra suggest that the equilibrium structures of the anions are significantly different from the neutrals. The PE spectrum of $C_6F_5Cl^-$ exhibits a parallel PAD, similar to that of the $C_6F_6^-$ spectrum, while the PE spectra of $C_6F_5Br^-$ and $C_6F_5I^-$ have isotropic PADs, and are both punctuated by the presence of their respective X^- atomic anion PE spectra. Identification of the detachment transition origin, which would correspond to the neutral EA, is difficult because of vanishingly small Franck-Condon overlap near the origin. Upper limits on the EAs were determined to be 1.70 eV for C_6F_5Cl, 2.10 eV for C_6F_5Br, and 2.00 eV for C_6F_5I. The VDE observed in the $C_6F_5Cl^-$ spectrum was 2.95 eV, while the VDEs for the other two species lie between 3.15 eV and 3.45 eV.

The computational results suggest that the primary difference between the structures of the anions and their respective neutrals is the C–X bond length, which is markedly longer in the anions. In contrast to the $C_6F_6^-$ anion, in which the excess charge is delocalized over the ring of the non-planar anion, the SOMO in $C_6F_5X^-$ (X = Cl, Br, I) is the local C–X σ* orbital. In $C_6F_5Cl^-$, the C–Cl bond is bent significantly out of the plane, while both the $C_6F_5Br^-$ and $C_6F_5I^-$ anions are predicted to be planar on average. For the $C_6F_5Br^-$ and $C_6F_5I^-$ anions, the SOMO, which is the orbital associated with the detachment transition, has significant 4p and 5p character for X = Br, I, respectively, which is consistent with the isotropic PAD. We suggest specific $\sigma^* \leftarrow \pi$ or $\sigma^* \leftarrow \sigma$ transitions that may result in photodissociation of $C_6F_5Br^-$ and $C_6F_5I^-$, leading to the observation of Br^- and I^- detachment signal observed in the PE spectra of the respective parent ions. The parallel PAD observed in the C $C_6F_5Cl^-$ PE spectrum is less easily reconciles with the significant 3p character of the SOMO, though it is distinct from the SOMO of the other two species in that it does not lie in the C_6 plane.

Detachment power studies are consistent with a two-photon (dissociation + X^- detachment) for $C_6F_5Br^-$, while for $C_6F_5I^-$, stimulated emission may be in competition with photodissociation.

A synthesis of the computational results suggests that the C–X bond in all three cases (X = Cl, Br, I) is has covalent character, in contrast with the more polar C–F bonds.

ASSOCIATED CONTENT

Supporting Information

The Supporting Information is available free of charge at https://pubs.acs.org/doi/10.1021/acs.jpca.XXXX

The Supporting Information includes raw and reconstructed photoelectron images, PAD-integrated PE spectra of the anions obtained using 3.495 eV and 2.330 eV (for $C_6F_5Br^-$ and $C_6F_5I^-$), detailed structures of C_6F_5X (X = Cl, Br, I) neutrals and anions from new calculations presented here, detailed structures and valence orbital isosurfaces/energies for C_6F_5X (X = F, Cl, Br) anions and neutrals using methods used previously[34] on $C_6F_6/C_6F_6^-$ for direct comparison with previous and current computations, MBIS atom charges for anions and neutrals (X = F, Cl, Br, I), APT charges of the anions and neutrals, (X = Cl, Br), and computed dipole moments of C_6F_5X (X = Cl, Br, I).

AUTHOR INFORMATION

Corresponding Author

Caroline Chick Jarrold - Department of Chemistry, Indiana University, 800 E. Kirkwood Avenue, Bloomington, Indiana 47405, United States; http://orcid.org/0000-0001-9725-4581; Email: cjarrold@indiana.edu

Authors

Kristen Rose McGinnis - Department of Chemistry, Indiana University, 800 E. Kirkwood Avenue, Bloomington, Indiana 47405, United States; https://orcid.org/0000-0001-8630-7166; Email: krrmcgin@iu.edu

Conor J. McGee - Department of Chemistry, Indiana University, 800 E. Kirkwood Avenue, Bloomington, Indiana 47405, United States; https://orcid.org/0009-0007-8563-0720; Email: comcgee@iu.edu

Thomas Sommerfeld - Department of Chemistry and Physics, Southeast Louisiana University, SLU 10878, Hammond, Louisiana 70402, United States; http://orcid.org/0000-0001-8105-5414; Email: thomas.sommerfeld@selu.edu

Notes

The authors declare no competing financial interest.

ACKNOWLEDGEMENTS

The authors gratefully acknowledge support from the National Science Foundation under Grant No. 2053889.

References

[1] Xue, T.; Dixon, A. R.; Sanov, A. Anion Photoelectron Imaging Spectroscopy of Glyoxal. *Chem. Phys. Lett.* **2016**, *660*, 205– 208.

[2] Dauletyarov, Y.; Dixon, A. R.; Wallace, A. A.; Sanov, A. Electron Affinity and Excited States of Methylglyoxal. *J. Chem. Phys*. **2017**, *147*, No. 013934.

[3] Dauletyarov, Y.; Wallace, A. A.; Blackstone, C. C.; Sanov, A. Photoelectron Spectroscopy of Biacetyl and Its Cluster Anions. *J. Phys. Chem. A* **2019**, *123*, 4158– 4167.

[4] Dobulis, M. A.; McGee, C. J.; Sommerfeld, T.; Jarrold, C. C. Autodetachment over Broad Photon Energy Ranges in the Anion Photoelectron Spectra of $[O_2\text{-}M]^-$ (M = Glyoxal, Methylglyoxal, or Biacetyl) Complex Anions. *J. Phys. Chem. A* **2021**, *125*, 9128-9142.

[5] Dobulis, M.A.; Thompson, M.C.; Jarrold, C.C. Identification of Isoprene Oxidation Reaction Products via Anion Photoelectron Spectroscopy. *J. Chem. Phys. A* **2021**, *125*, 10089-10102.

[6] Shuman, N.S.; Friedman, J.F.; Miller, T.M.; Viggiano, A.A. Electron Attachment to 14 Halogenated Alkenes and Alkanes, 300-600K. *Chem. Phys*. **2012**, *137*, 164306.

[7] Williams, B. A.; Siedle, A. R.; Jarrold, C. C. Identification of Stable Perfluorocarbons Formed by Hyperthermal Decomposition of Graphite Fluoride Using Anion Photoelectron Spectroscopy. *J. Phys. Chem. C* **2022**, *126,* 9965-9978.

[8] Miller, T.M.; Friedman, J.F.; Shuman, N.S.; Ard, S.G.; Melko, J.J.; Viggiano, A.A. Electron Attachment to C_7F_{14}, Thermal Detachment from $C_7F_{14}^-$, the Electrom Affinity of C_7F_{14}, and Neutralization of $C_7F_{14}^-$ by Ar^+. *J. Phys. Chem. A* **2012**, *116*, 10293-10300.

[9] Van Doren, J.M.; Condon, L.R.; DeSouza-Goding, A.; Miller, T.M.; Bopp, J.C.; Viggiano, A.A. Electron Affinity of *trans*-2-C_4F_8 from Electron Attachment-Detachment Kinetics. *J. Phys. Chem. A* **2010**, *114*, 1420-1426.

[10] Bopp, J.C.; Roscioli, J.R.; Johnson, M.A.; Miller, T.M.; Viggiano, A.A.; Villano, S.M.; Wren, S.W.; Lineberger, W.C. Spectroscopic Characterization of the Isolated SF_6^- and $C_4F_8^-$ anions: Observation of Very Long Harmonic Progressions in Symmetric Deformation Modes upon Photodetachment. *J. Phys. Chem. A* **2007**, *111*, 1214-1221.

[11] Van Doren, J.M.; Kerr, D.M.; Miller, T.M.; Viggiano, A.A. Electron Attachment and Detachment, and the Electron Affinitites of C_5F_5N and C_5HF_4N. *J. Chem. Phys*. **2005**, *123*, 114303.

[12] King, R.A.; Pettigrew, N.D.; Schaefer, H.F. The Electron Affinities of the Perfluorocarbons, C_2F_n, n = 1-6. J. Chem. Phys. **1997**, *107*, 8536-8544.

[13] Van Dporen, J.M.; McSweeney, S.A.; Hargus, M.D.; Kerr, D.M.; Miller, T.M.; Arnold, S.T. Viggiano, A.A. Electron Attachment and Detachment: cyclo-$C_4F_4Cl_2$. *Int. J. Mass Spec*. **2003**, *228*, 541-549.

[14] Brinkmann, N.R.; Rienstra-Kiracofe, J.C.; Schaefer III, H.F. Electron Affinities of Cyano-Substituted Ethylenes. *Mol. Phys*. **2001**, *99*, 663-675.

[15] Ranković, M.; Nag, P.; Anstöter, C.S.; Mensa-Bonsu, G.; Kumar, T.P.R.; Verlet, J.R.R.; Fedor, J. Resonances in Nitrobenzene Probed by the Electron Attachment to Neutral and by the Photodetachment from Anion. *J. Chem. Phys*. **2022**, *157*, 064302.

[16] Chowdhury, S.; Kishi, H.; Dillow, G.W.; Kebarle, P. Electron Affinities of Substituted Nitrobenzenes. *Can. J. Chem.* **2989**, *67*, 603-610.

[17] Chen, G.; Cooks, G.R. Electron Affinities of Polycyclic Aromatic Hydrocarbons Determined by the Kinetic Method. *J. Mass Spec.* **1995**, *30*, 1167-1173.

[18] Kregel, S.J.; Thurston, G.K.; Garand, E. Photoelectron Spectroscopy of Anthracene and Fluoranthene Radical Anions. *J. Chem. Phys*. **2018**, *148*, No. 234306.

[19] Jalehdoost, A.; von Issendorff, B. photon Energy Dependene of the Photoelectron Spectra of the Anthracene Anion: On the Influence of Autodetaching States. *J. Chem. Phys.* **2023**, *158*, No. 194302.

[20] Mitsui, M.; Ando, N.; Nakajima, A.; Mass Spectrometry and Photoelectron Spectroscopy of Tetracene Cluster Anions, $(Tetracene)_n^-$ (n = 1-100): Evidence for the Highly Localized Nature of Polarizatino in a Cluster Analogue of Oligoacene Crystals, *J. Phys. Chem. A* **2007**, *111*, 9644-9648.

[21] Sagan, C.R.; Anstöter, C.S.; Thodika, M.; Wilson, K.D.; Matsika, S.; Garand, E. Spectroscopy and Theoretical Modeling of Tetracene Anion Resonances. *J. Phys. Chem. Lett.* **2022**, *13*, 10245-10252.

[22] Heinis, T.; Chowdhury, S.; Kebarle, P. Electron Affinities of Napthalene, Anthracene, and Substituted Napthalenes and Anthracenes. *Org. Mass Spec*. **1993**, *28*, 358-365.

[23] Crocker, L.; Wang, T.; Kebarle, P. Electron Affinities of some Polycyclic Aromatic Hydrocarbons, Obtained from Electron-Transfer Equilibria. *J. Am. Chem. Soc.* **1993**, *115*, 7818-7822.

[24] Chowdhury, S.; Grimsrud, E.P.; Heinis, T.; Kebarle, P. Electron Affinities of Perfluorobenzene and Perfluorophenyl Compounds. *J. Am. Chem. Soc*. **1986**, *108*, 3630-3035.

[25] Lifshitz, C.; Tiernan, T.O.; Hughes, B.M. Electron Affinities from Endothermic Negative-Ion Charge-Transfer Reactoins. IV. SF_6, Selected Fluorocarbons and other Polyatomic Molecules. *J. Chem. Phys*. **1973**, *59*, 3182-3192.

[26] Miller, T.M.; Van Doren, J.M.; Viggiano, A.A. Electron Attachment and Detachment: $C_6F_6^-$. *Int. J. Mass Spec.* **2004**, *233*, 67-73.

[27] Rains, L.J.; Moore, J.W.; McIver Jr., R.T. Equilibrium Electron-Transfer Reactoins in the Gas Phase Involving Long-Lived Negative Ion Radicals. J. chem. Phys. **1978**, 68, 3309-3311.

[28] Spyrou, S.M.; Christophorou, L.G.; Effect of Temperature on Nondissociative Electron Attachment to Perfluorobenzene. J. Chem. Phys. **1985**, *82*, 1048-1049.

[29] McDonald, R.N.; Chowdhury, A.K.; Setser, D.W. Gas-Phase Ion-Molecule Reactoins of Cyclopentadienyl Anion ($c\text{-}C_5H_5^-$). J. Am. Chem. Soc. **1981**, *103*, 7586-7589.

[30] Knighton, W.B.; Bognar, J.A.; Grimsrud, E.P. Thermal Electro Detachment Rate Constants for the Molecular Anion of Perfluorobenzene, *Chem. Phys. Lett*. **1992**, *192*, 522-531.

[31] Eustis, S. N.; Wang, D.; Bowen, K. H.; Naresh Patwari, G. Photoelectron spectroscopy of hydrated hexafluorobenzene anions. *J. Chem. Phys.* **2007**, *127*, No. 114312.

[32] Rogers, J. P.; Anstöter, C. S.; Bull, J. N.; Curchod, B.F.E.; Verlet, J. R. R. Photoelectron Spectroscopy of the Hexafluorobenzene Cluster Anions: $(C_6F_6)_n^-$ (n = 1–5) and I^- (C_6F_6). *J. Phys. Chem. A* **2019**, *123*, 1602-1612.

[33] Nakajima, A.; Taguwa, T.; Hoshino, K.; Sugioka, T.; Naganuma, T.; Oho, F.; Watanabe, K.; Nakao, K.; Konishi, Y.; Kishi, R.; Kaya, K.Photoelectron Spectroscopy of $(C_6F_6)_n^-$ and $(Au\text{-}C_6F_6)^-$ Clusters. *Chem. Phys. Lett.* **1993**, *214*, 22–26.

[34] McGee, C.J.; McGinnis, K.R.; Jarrold, C.C. Anion Photoelectron Imaging Spectroscopy of C_6HF_6, C_6F_6, and the Absence of $C_6H_2F_4^-$. *J. Phys. Chem. A* **2023**, *127*, 8556-8565.

[35] Rogers, J.P.; Anstoter, C.S.; Verlet, J.R.R. Ultrafast Dynamics of Low-Energy Electron Attachment via a Non-Valence Correlation-Bound State. *Nat. Chem.* **2018**, *10*, 341-356.

[36] Voora, V. K.; Jordan, K. D. Nonvalence Correlation-Bound Anion State of C_6F_6: Doorway to Low-Energy Electron Capture. *J. Phys. Chem. A* **2014**, *118*, 7201-7205.

[37] Dillow, G.W.; Kebarle, P. Substituent Effects on the Electron Affinities of Perfluorobenzenes C_6F_5X. *J. Am. Chem. Soc.* **1989**, *111*, 5592-5596.

[38] Miller, T.M.; Viggiano, A.A. Electron Attachment and Detachment: C_6F_5Cl, C_6F_5Br, and C_6F_5I and the Electron Affinity of C_6F_5Cl. *Phys. Rev. A* **2005**, *71*, 012702.

[39] Chen, H.; Wang, R.; Xu, J.; Yuan, X.; Zhang, D.; Zhu, Z.; Marshall, M.; Bowen, K.; Zhang, X. Spontaneous Reduction by One Electron on Water Microdroplets Facilitates Direct Carboxylation with CO_2. *J. Am. Chem. Soc*. **2023***, 145*, 2647 – 2652.

[40] Mann, J.E.; Troyer, M.E.; Jarrold, C.C., Photoelectron Imaging and Photodissociation of Ozonide in $O_3^-\cdot(O_2)_n$ (n = 1 – 4). *J. Chem. Phys*. **2015**, *142*,124305.

[41] Bakker, J.M.B. A Beam-Modulatd Time-of-Flight Mass Spectrometer. I. Theoretical Considerations. *J. Phys. E.* **1973**, *6*, 785-789.

[42] Bakker, J.M.B Beam-Modulated Time-of-Flight Mass-Spectrometer. 2. Experimental Work. *J. Phys. E* **1974**, *7*, 364-368.

[43] Chandler, D. W.; Houston, P. L. Two-dimensional imaging of state-selected photodissociation products detected by multiphoton ionization. *J. Chem. Phys.* **1987**, *87*, 1445-1447.

[44] Eppink, A.T.J.B.; Parker, D.H. Velocity Map Imaging of Ions and Electrons using Electrostatic Lenses: Application in Photoelectron and Photofragment Ion Imaging of Molecular Oxygen. *Rev. Sci. Instrum.* **1997**, *68*, 3477-3484.

[45] Sanov, A.; Mabbs, R. Photoelectron imaging of negative ions. *Int. Rev. Phys. Chem.* **2008**, *27*, 53-85.

[46] Doyle, M. B.; Abeysekera, C.; Suits, A. G. NuAcq 0.9: Native Megapixel Ion Imaging with Centroiding to 4 Mpix Using Inexpensive USB-2 Cameras. Available at http://faculty.missouri.edu/suitsa/NuAqc.html. (accessed February 4, 2020)

[47] Dribinski, V.; Ossadtchi, A.; Mandelshtam, V. A.; Reisler, H. Reconstruction of Abel-Transformable Images: The Gaussian Basis-Set Expansion Abel Transform Method. *Rev. Sci. Instrum.* **2002**, *73*, 2634– 2642,

[48] Garcia, G.A.; Nahon, L.; Powis, I. Two-Dimensional Charged Particle Image Inversion Using a Polar Basis Function Expansion. *Rev. Sci. Instrum*. **2004**, 75, 4989-4996.

[49] Ervin, K. M.; Anusiewicz, I.; Skurski, P.; Simons, J.; Lineberger, W. C. The Only Stable State of O_2^- is the $X^2\Pi_g$ Ground State and It (Still!) Has an Adiabatic Electron Detachment Energy of 0.45 eV. *J. Phys. Chem. A* **2003**, *107*, 8521– 8529.

[50] Chai, J.-D.; Head-Gordon, M. Long-range corrected hybrid density functionals with damped atom–atom dispersion corrections, *Phys. Chem. Chem. Phys*. **2008**, *10*, 6615–6620.

[51] Rappoport, D.; Furche, F. Property-optimized Gaussian basis sets for molecular response calculations, *J. Chem. Phys.* **2010**, *133*, 134105.

[52] Peterson, K.A.; Figgen, D.; Goll, E.; Stoll, H.; Dolg, M. Systematically Convergent Basis Sets with Relativistic Pseudopotentials.: II.: Small-Core Pseudopotentials and Correlation Consisten Basis Sets for the Post-d Group 16-18 Elements. *J. Chem. Phys*. **2023**, *119*, 11113-11123.

[53] Stoychev, G. L.; Auer, A. A.; Neese, F.; Automatic Generation of Auxiliary Basis Sets. *J. Chem. Theor. Comp.* **2017,** *13*, 554-562.

[54] Dunning, T. H., Jr. Gaussian basis sets for use in correlated molecular calculations. I. The atoms boron through neon and hydrogen. *J. Chem. Phys.* **1989**, *90*, 1007-1023.

[55] Riplinger, C.; Neese, F. An efficient and near linear scaling pair natural orbital based local coupled cluster method, *J. Chem. Phys*. **2013**, *138,* 034106.

[56] Karton, A.; Tarnopolsky, A.; Lamere, J.-F.; Schatz, G.C.; Martin, J.M.L. Highly Accurate First-Principles Benchmark Data Sets for the Parametrization and Validation of Density Functional and Other Approximate Methods. Derivation of a Robust, Generally Applicable, Double-Hybrid Functional for Thermochemistry and thermochemical Kinetics. *J. Phys. Chem. A* **2008**, *112*, 12868-12886.

[57] Neese, F.; Wennmohs, F.; Becker, U.; Riplinger, C. The ORCA Quantum Chemistry Program Package. *J. Chem. Phys.* **2020**, *152*, 224108.

[58] Verstraelen, T.; Vandenbrande, S.; Heidar-Zadeh, F.; Vanduyfhuys, L.; Van Speybroeck, V.; Waroquier, M.; Ayers, P.S. Minimal Basis Iterative Stockholder: Atoms in Molecules for Force-Field Development. *J. Chem. Theory Comp*. **2016**, *12*, 3894-3912.

[59] Davis, J. U.; Chick Jarrold, C.; Sommerfeld, T. Charge Distribution in Oxygen·fluorobenzene Complex Anions $[O_2{\cdot}C_6H_{6-n}F_n]^-$ (n = 0 – 6). *Chem. Phys.* **2023**, *574*, 112023.

[60] Becke, A. D. Density-Functional Exchange-Energy Approximation with Correct Asymptotic Behavior. *Phys. Rev. A* **1988**, *38*, 3098–3100.

[61] Lee, C.; Yang, W.; Parr, R.G. Milestone Development of the Colle-Salvetti Correlation-Energy Formula into a Functional of the Electron Density. *Phys. Rev. B*, **1988**, *37*, 785–789.

[62] Becke, A. D. Density-Functional Thermochemistry. III. The Role of Exact Exchange. *J. Chem. Phys*. **1993**, *98*, 5648–5652.

[63] Woon, D.E.; Dunning, Jr., T.H. Gassian Basis Sets for Use in Correlated Molecular Calculations. III. The Atoms Aluminum through Argon. *J. Chem. Phys*. **1993**, *98*, 1358-1371.

[64] Wilson, A.K.; Woon, D.E.; Peterson, K.A.; Dunning, Jr. T.H. Gaussian Basis Sets for Use in Correlated Molecular Calculations. IX. The Atoms Gallium through Krypton. *J. Chem. Phys.* **1999**, *110*, 7667-7676.

[65] M. J. Frisch, G. W. Trucks, H. B. Schlegel, G. E. Scuseria, M. A. Robb, J. R. Cheeseman, G. Scalmani, V. Barone, G. A. Petersson, H. Nakatsuji, *et al*. Gaussian 16, Gaussian Inc., Wallingford, CT, USA, 2016.

[66] Williams, B. A.; Siedle, A. R.; Jarrold, C. C. Evidence of CF_2 Loss from Fluorine-Rich Cluster Anions Generated from Laser Ablation of Graphite Fluoride. *J. Phys. Chem. A* **2018**, *122*, 9894-9900.

[67] Zare, R.N. Photoejection Dynamics [1]. *Mol. Photochem*. **1972**, *4*, 1-37.

[68] Cooper, J.; Zare, R.N. Angular Distribution of Photoelectrons. *J. Chem. Phys.* **1968**, *48*, 942-943.

[69] Cooper, J.; Zare, R.N. Erratum: Angular Distribution of Photoelectrons. *J. Chem. Phys.* **1968**, *49*, 4252

[70] Sanov, A. Laboratory-Frame Photoelectron Angular Distributions in Anion Photodetachment: Insight into Electronic Structure and Intermolecular Interactions. *Annu. Rev. Phys. Chem.* **2014**, *65*, 341– 363.

[71] Khuseynov, D.; Blackstone, C.C.; Culberson, L.M.; Sanov, A. Photoelectron Angular Distributions for States of any Mixed Character: An Experiment-Friendly Model for Atomic, Molecular, and Cluster Anions. *J. Chem. Phys.* **2014**, *141*, 124312.

[72] Wigner, E.P. On the Behavior of Cross Sections Near Thresholds. *Phys. Rev.* **1948**, *72*, 1002-1009.

[73] Price, S. J. W.; Sapiano, H. J. C_6F_5X Bond Dissociation Energies: Determination from Appearance Potential Measurements and Correlation with Thermochemical Data. *Can. J. Chem.* **1974**, *52*, 4109-4111.

[74] "Bond Dissociation Energies," in CRC Handbook of Chemistry and Physics, 104th Edition (Internet Version 2023), John R. Rumble, ed., CRC Press/Taylor & Francis, Boca Raton, FL.

[75] McGee, C.J.; McGinnis, K.R.; Jarrold, C.C. Trend in the Electron Affinities of Fluorophenyl Radicals $\cdot C_6H_{5-x}F_x$ ($1 \leq x \leq 4$). *J. Phys. Chem. A* **2023**, *127*, 7264-7273.

[76] Rienstra-Kiracofe, J.C.; Tschumper, G.S.; Schaefer III, H.F.; Nandi, S.; Ellison, G.B. Atomic and Molecular Electron Affinities: Photoelectron Experiments and Theoretical Computations. *Chem. Rev*. **2002**, *102*, 231-383.

[77] Continetti, R.E.; Guo, H. Dynamics of Transient Species via Anion Photodetachment. *Chem. Soc. Rev*. **2017**, *46*, 7650-7667.

[78] Benitez, Y.; Nguyen, T.L.; Parsons, A.J.; Stanton, J.F.; Continetti, R.E. Probing the Exit Channel of the $OH + CH_3OH \rightarrow H_2O + CH_3O$ Reaction by Photodetahment of $CH_3O^-(H_2O)$. *J. Phys. Chem. Lett*. **2022**, *13*, 142-148.

[79] Continetti, R.E. Photoelectron-Photofragment Coincidence Studies of Dissociation Dynamics. *Int. Rev. Phys. Chem.* **1998**, *17*, 227-260.

[80] Gibbard, J.A.; Continetti, R.E. Photoelectron Photofragment Coincidence Spectroscopy of Carboxylates. *RSC Adv*. **2021**, *11*, 34250-34261.

[81] "Dipole Moments," in CRC Handbook of Chemistry and Physics, 104th Edition (Internet Version 2023), John R. Rumble, ed., CRC Press/Taylor & Francis, Boca Raton, FL.

[82] Tantardini, C.; Oganov, A.R. Thermochemical Electronegativities of the Elements. *Nat. Comm*. **2021**, *12,* 2087.

[83] Mulliken, R.S.; A New Electron Affinity Scale; Together with Data on Valence States and on Valence Ionizatino Potentials and Electron Affinities. *J. Chem. Phys*. **1934**, *2*, 782-793.

[84] Alabugin, I. V.; Bresch, S.; Manoharan, M. Hybridization Trends for Main Group Elements and Expanding the Bent's Rule beyond Carbon: More than Electronegativity. *J. Phys. Chem. A* **2014**, *118*, 3663–3677.

[85] Cao, C.-T.; Chen, M.; Fang, Z.; Au, C.; Cao, C. Relationship Investigation between C(sp_2)–X and C(SP3)–X Bond Energies Based on Substituted Benzene and Methane. *ACS Omega* **2020**, *5*, 19304–19311.

LIST OF FIGURES

Table 1. Results of calculations on the EA and VDE values calculated for $C_6F_6^-$, $C_6F_5Cl^-$, $C_6F_5Br^-$, and $C_6F_5I^-$, along with experimental EA and VDE values. Note that the experimental EA values represent an upper limit on the actual EA, since the transition intensity at the origin may be vanishingly small.

Molecule	Computational method/basis set	EA	VDE	Exp. EA/VDE (eV)
C_6F_6	ωB97X/def2-TZVPPD	0.38	1.45	
	DLPNO-CCSD(T)/aug-cc-pVTZ//ωB97X	0.41	1.35	
	B2GBLYP/aug-cc-pVTZ	0.42	1.32	< 0.76 / 1.60 ± 0.05 eV
	DLPNO-CCSD(T)/aug-cc-pVTZ//B2GBLYP	0.38	1.21	
C_6F_5Cl	ωB97X/def2-TZVPPD	0.72	3.36	
	DLPNO-CCSD(T)/aug-cc-pVTZ//ωB97X	0.70	2.96	< 1.70 / 2.95 ± 0.05
	B2GBLYP/aug-cc-pVTZ	0.80	3.04	
	DLPNO-CCSD(T)/aug-cc-pVTZ//B2GBLYP	0.68	2.82	
C_6F_5Br	ωB97X/def2-TZVPPD	1.09	3.34	
	DLPNO-CCSD(T)/aug-cc-pVTZ//ωB97X	0.97	2.81	< 2.10 / 3.15 – 3.45
	B2GBLYP/ SK-MCDHF-RSC ECP	1.09	2.99	
	DLPNO-CCSD(T)/ SK-MVDHF-RSC ECP //B2GBLYP SK-MVDHF-RSC ECP	0.96	2.81	
C_6F_5I	ωB97X/def2-ECP	1.38	3.18	
	DLPNO-CCSD(T)/aug-cc-pVTZ//ωB97X	--	--	< 2.00 / 3.15 – 3.45
	B2GBLYP/SK-MCDHF-RSC ECP	1.37	2.90	
	DLPNO-CCSD(T)/ SK-MVDHF-RSC ECP //B2GBLYP SK-MVDHF-RSC ECP	1.23	2.73	

Table 2. Summary of bond dissociation energies of H_5C_6–X (X = CH_3, H, F, Cl, Br, I) from Ref. 74 along with the bond dissociation energy of F_5C_6–X, (X = H, F, Cl, Br, I) from Ref.73. Atomic EAs are from Ref. 76.

X	BDE H_5C_6-X	BDE F_5C_6-X	EA of X
H	4.83 eV	5.05 eV	0.754 eV
F	5.51 eV	6.52 eV	3.339 eV
Cl	4.21 eV	5.51 eV	3.617 eV
Br	3.57 eV	4.59 eV	3.365 eV
I	2.85 eV	2.87 eV	3.059 eV

Table 3. Difference in MBIS atom charges for C_6F_5X (X = F, Cl, Br, I) neutral and anionic molecules (Δq = anion – neutral) using ωB97X/def2-TZVPPD, along with Loewdin spin populations (SP) in the double anions from B2GBLYP/aug-cc-pVTZ. Numbers in boldface are the unique carbon center, C_X, and X atoms in the C_6F_5X (X = Cl, Br, I) anions and neutrals. In the case of C_6F_6, the two identical C centers in the C_{2v} anion and their associated F atoms are in bold face. Raw MBIS atom charges for all atoms are include in the **Supporting Information**.

	C_6F_6 Δq / SP	C_6F_5Cl Δq / SP	C_6F_5Br Δq / SP	C_6F_5I Δq / SP
C_X	**-0.23 / 0.223**	**-0.06 / 0.415**	**-0.02 / 0.406**	**-0.02 / 0.374**
C_α	-0.02 / 0.084	-.02 / 0.064	-0.03 / 0.040	-0.03 / 0.034
C_β	-0.02 / 0.084	-.02 / 0.021	-0.03 / 0.032	-0.04 / 0.028
C_γ	**-0.23 / 0.223**	-.04 / -0.004	-0.04 / -0.027	-0.04 / -0.025
X	**-0.08 / 0.061**	**-0.58 / 0.392**	**-0.60 / 0.457**	**-0.62 / 0.512**
F_α	-0.07 / 0.024	-0.05 / 0.005	-0.05 / -0.002	-0.04 / -0.002
F_β	-0.07 / 0.024	-0.05 / 0.010	-0.04 / 0.016	-0.04 / 0.014
F_γ	**-0.08 / 0.061**	-0.04 / 0.003	-0.04 / -0.011	-0.04 / 0.010

MBIS atom charges for C_X and X in neutral C_6F_5X

C_X	0.127	-0.115	-0.198	-0.337
X	-0.127	-0.052	-0.002	0.077

MBIS atom charges for C_X and X in $C_6F_5X^-$

C_X	-0.104[a] ; 0.106[b]	-0.170	-0.222	-0.354
X	-0.202	-0.629	-0.600	-0.540

[a] MBIS atom charge on the two identical C atoms in the C_{2v} structure

[b] MBIS atom charges on the four identical C atoms in the C_{2v} structure.

TOC Graphic

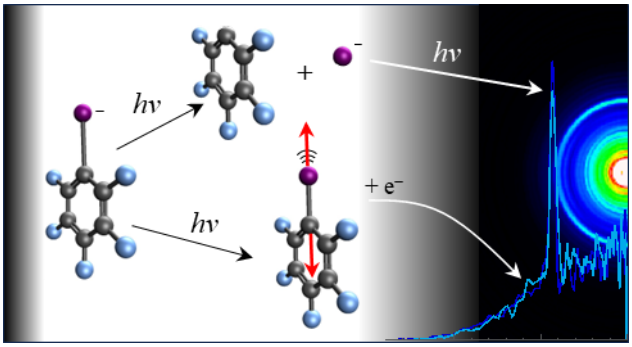

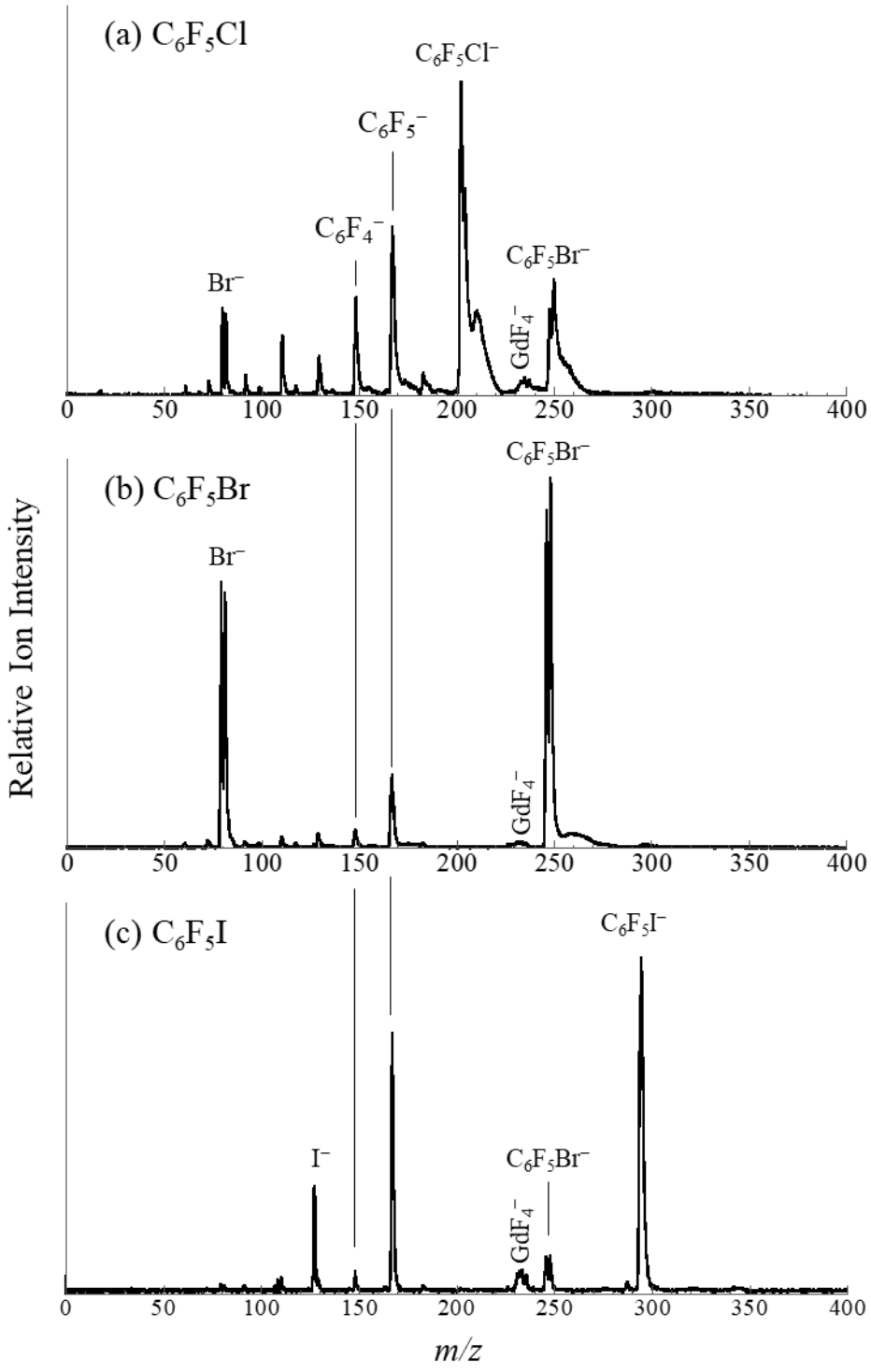
(a) C_6F_5Cl
$C_6F_5Cl^-$
$C_6F_5^-$
$C_6F_4^-$
$C_6F_5Br^-$
Br^-
GdF_4^-
(b) C_6F_5Br
$C_6F_5Br^-$
Br^-
GdF_4^-
(c) C_6F_5I
$C_6F_5I^-$
I^-
$C_6F_5Br^-$
GdF_4^-
Relative Ion Intensity
0 50 100 150 200 250 300 350 400
m/z

Figure 1

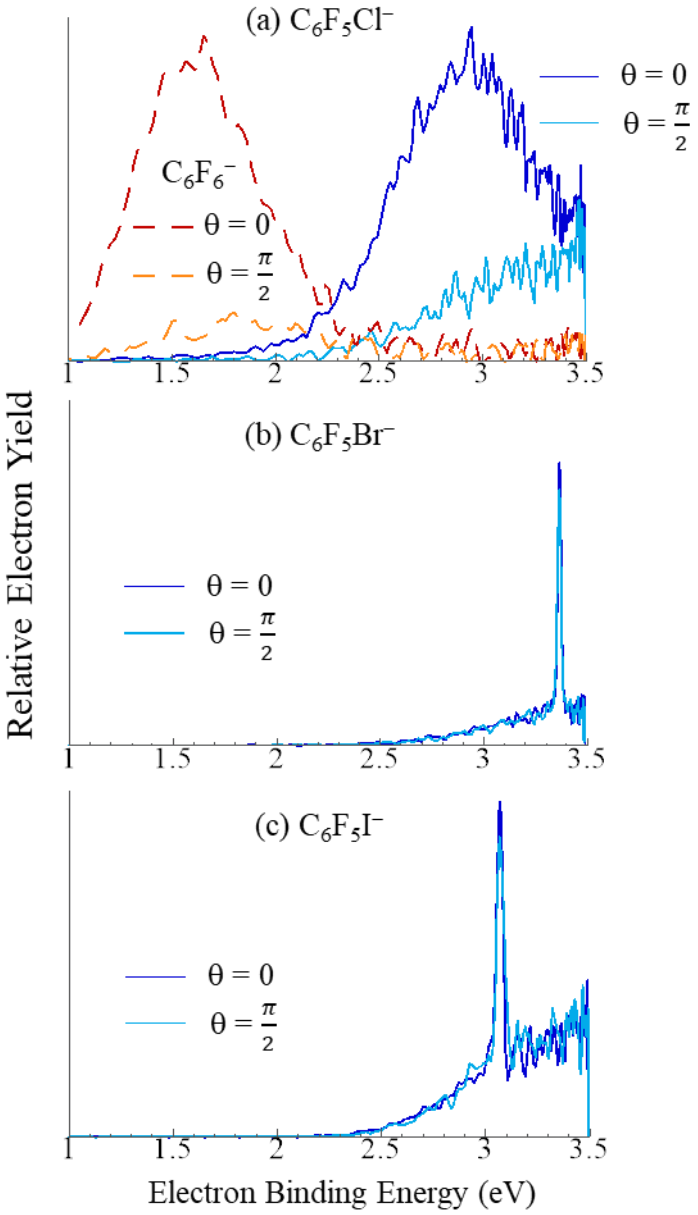
(a) $C_6F_5Cl^-$
$C_6F_6^-$
θ = 0
θ = π/2
θ = 0
θ = π/2
(b) $C_6F_5Br^-$
θ = 0
θ = π/2
(c) $C_6F_5I^-$
θ = 0
θ = π/2
1
1.5
2
2.5
3
3.5
Relative Electron Yield
Electron Binding Energy (eV)

Figure 2

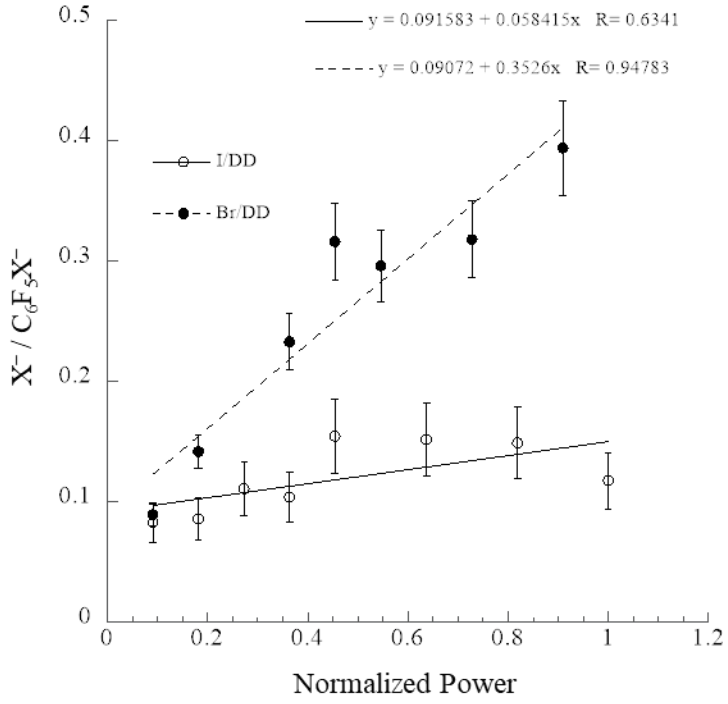
y = 0.091583 + 0.058415x R= 0.6341
y = 0.09072 + 0.3526x R= 0.94783
I/DD
Br/DD
X⁻ / C6F5X⁻
Normalized Power
0
0.1
0.2
0.3
0.4
0.5
0.2
0.4
0.6
0.8
1
1.2

Figure 3

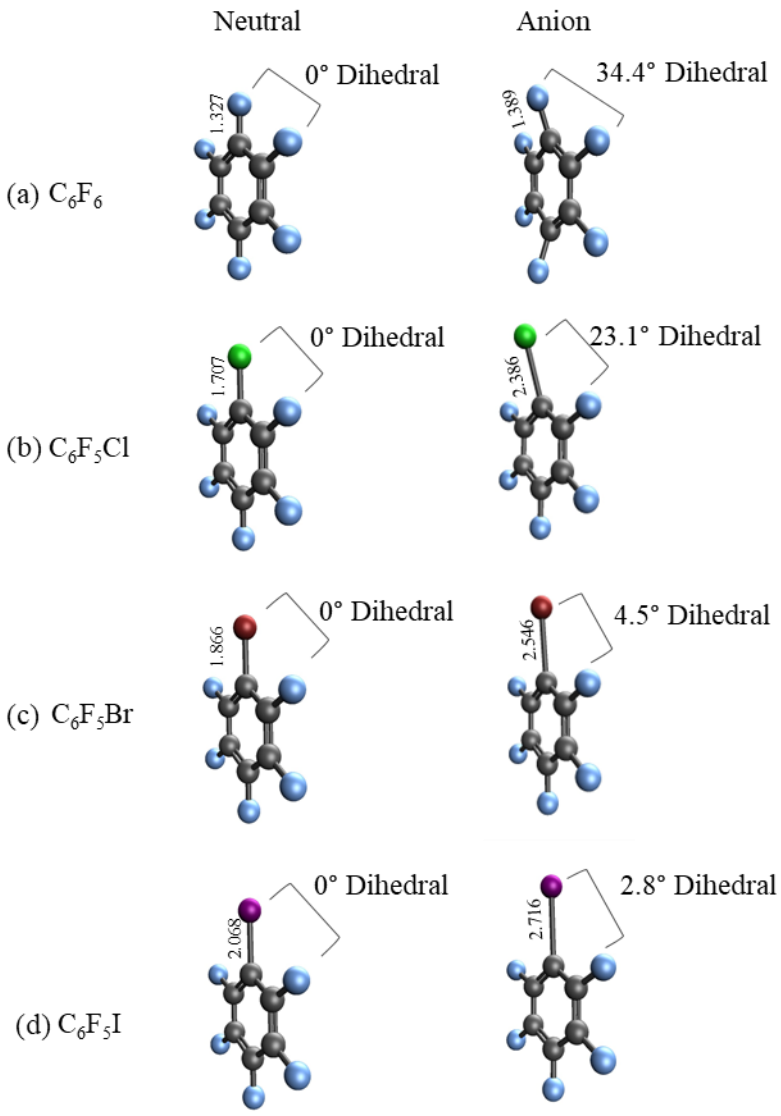
Neutral
Anion
(a) C_6F_6
0° Dihedral
1.327
34.4° Dihedral
1.389
(b) C_6F_5Cl
0° Dihedral
1.707
23.1° Dihedral
2.386
(c) C_6F_5Br
0° Dihedral
1.866
4.5° Dihedral
2.546
(d) C_6F_5I
0° Dihedral
2.068
2.8° Dihedral
2.716

Figure 4

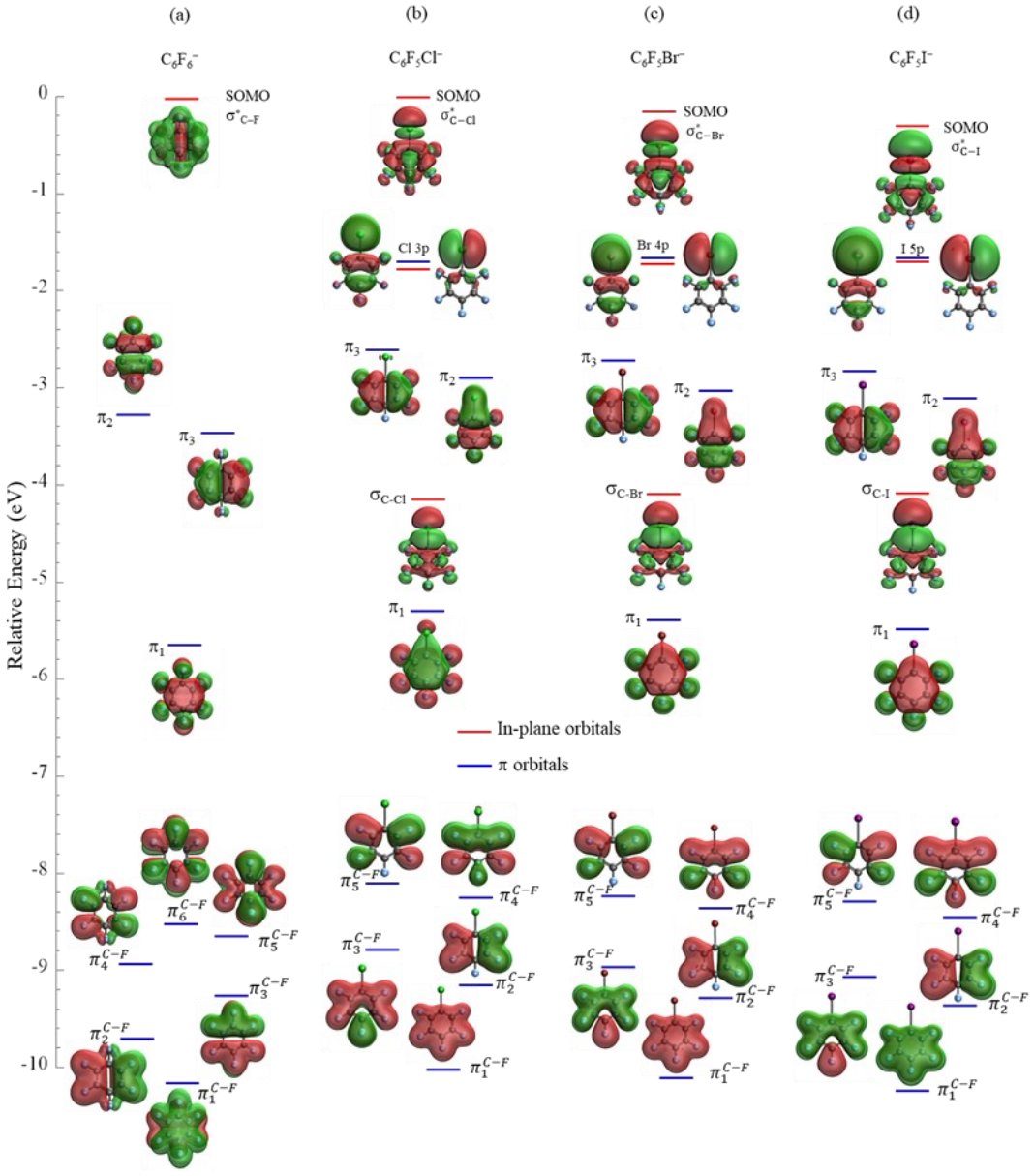
(a)
(b)
(c)
(d)
$C_6F_6^-$
$C_6F_5Cl^-$
$C_6F_5Br^-$
$C_6F_5I^-$
SOMO
σ^*_{C-F}
σ^*_{C-Cl}
σ^*_{C-Br}
σ^*_{C-I}
Cl 3p
Br 4p
I 5p
π_3
π_2
π_1
σ_{C-Cl}
σ_{C-Br}
σ_{C-I}
In-plane orbitals
π orbitals
Relative Energy (eV)
0
-1
-2
-3
-4
-5
-6
-7
-8
-9
-10
π_6^{C-F}
π_5^{C-F}
π_4^{C-F}
π_3^{C-F}
π_2^{C-F}
π_1^{C-F}

Figure 5

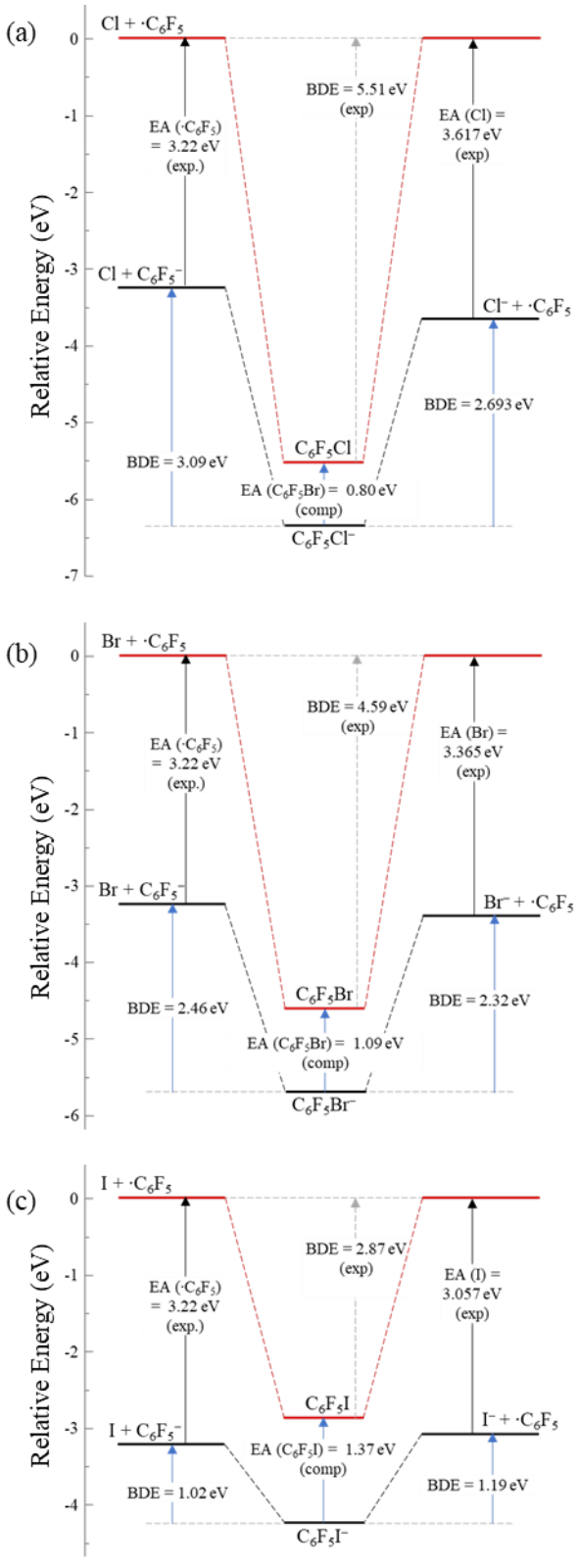
(a)
Cl + ·C6F5
EA (·C6F5) = 3.22 eV (exp.)
BDE = 5.51 eV (exp)
EA (Cl) = 3.617 eV (exp)
Cl + C6F5−
Cl− + ·C6F5
BDE = 3.09 eV
BDE = 2.693 eV
C6F5Cl
EA (C6F5Br) = 0.80 eV (comp)
C6F5Cl−
Relative Energy (eV)
0
-1
-2
-3
-4
-5
-6
-7
(b)
Br + ·C6F5
EA (·C6F5) = 3.22 eV (exp.)
BDE = 4.59 eV (exp)
EA (Br) = 3.365 eV (exp)
Br + C6F5−
Br− + ·C6F5
BDE = 2.46 eV
BDE = 2.32 eV
C6F5Br
EA (C6F5Br) = 1.09 eV (comp)
C6F5Br−
Relative Energy (eV)
0
-1
-2
-3
-4
-5
-6
(c)
I + ·C6F5
EA (·C6F5) = 3.22 eV (exp.)
BDE = 2.87 eV (exp)
EA (I) = 3.057 eV (exp)
I + C6F5−
I− + ·C6F5
C6F5I
EA (C6F5I) = 1.37 eV (comp)
BDE = 1.02 eV
BDE = 1.19 eV
C6F5I−
Relative Energy (eV)
0
-1
-2
-3
-4

Figure 6